Conf-9403151--2

Electron-Positron Pair Production in Ultrarelativistic Atomic Collisions: 6.4 TeV S^{16+} with Au, Pd and Al

S. Datz, C. R. Vane, P. F. Dittner, and H. F. Krause

Physics Division, Oak Ridge National Laboratory,
Oak Ridge, TN 38731

R. Schuch and H. Gao

Atomic Physics, Stockholm University, Frescativagen 24,
S-104 05 Stockholm 50, Sweden

R. Hutton

Atomic Spectroscopy, University of Lund, Department of Physics,
Sölvegatan 14, S-223 62 Lund, Sweden

ABSTRACT

Angular and momentum distributions have been measured for electron-positron pairs created in peripheral collisions of 6.4 TeV bare sulfur ions with thin targets of Al, Pd, and Au. Singly- and doubly-differential cross sections are presented for 1–17 MeV/c electrons and positrons detected independently and in coincidence as pairs. Various physical parameters are deduced from the coincident electron and positron data, including probability distributions for the pair transverse momentum, the pair total energy, and the positron fraction of the pair energy.

I. INTRODUCTION

Christopher Bottcher was a man full of surprises. When an interesting problem appealed to our experimentalist eyes, which seemed quite original, it was often true that on second examination one could find a seminal paper or two that Chris had written on the subject. Following the initial contact, he would join us in enthusiastic collaborations. This was certainly true in our work on dielectronic recombination from which a whole cottage industry has sprung. His name appears as a co-author of our (ORNL) first experimental paper [1] on the subject.

DISCLAIMER

Portions of this document may be illegible in electronic image products. Images are produced from the best available original document.

An almost parallel situation occured in regard to our work on ultrarelativistic collisions. In a short paper during a meeting on ion -atom collisions in Frankfurt in 1976, Bauer showed a graph which indicated rather large cross sections for pair production in heavy particle collisions as a function of gamma. Being aware of the ORNL participation in the CERN collaboration which utilized 200 GeV/amu S^{16+} beams to study quark-gluon plasmas, the possibilities of starting experiments in this area became interesting. Discovering later that theoretical predictions varied by two orders-of-magnitude excited ones experimentalist salivary glands. The greatest discovery, however, was that Chris Bottcher and Mike Strayer had been and were among the leading active theorists in the field. (GO FIGURE!) They worked intimately with us on both the steep and gradual portions of our learning curves and were included as co-authors in our first paper in this field.[2] What follows below is an abbreviated version of a paper which is to appear in Physical Review A.[3] We include it here to indicate the breadth of Chris's talents and the *spetzatura* with which he was able to make transitions between problems in widely varying areas.

Aside from our intrinsic interest in the physics of the pair production process, the results of this work can have strong implications for the next generation of heavy-ion machines. Recent progress toward realization of very energetic ion-ion colliders such as the Relativistic Heavy-Ion Collider (RHIC) at Brookhaven National Laboratory and the Large Hadron Collider (LHC) at CERN has sparked renewed interest in electromagnetic phenomena at very high energies. A number of theoretical treatments have recently appeared concentrating on lepton-pair production in ultrarelativistic heavy-ion collisions.[4-13] Results of these varied calculations differ substantially in quantitative detail, but generally agree that electron-pair production cross sections should be large, should steadily increase with collision energy, and should lead to

single- and possibly multiple-pair formation at rates sufficient to overwhelm contributions from all other processes. In particular, direct Coulomb pair production may obviate the suggested[6] use of lepton signals as a penetrating probe for studying formation and decay of the quark-gluon plasma in ultrarelativistic heavy-ion nuclear collisions.[14-16]

II. EXPERIMENTAL METHOD

Fully-stripped 6.4 TeV (200 GeV/nucleon) sulfur ions from the CERN Super Proton Synchrotron (SPS) accelerator were passed through thin foil targets in a high-vacuum chamber centered in the 14 cm gap of a 1 meter long, CERN standard dipole bending magnet located upstream of a large nuclear physics collaboration experiment WA93. A schematic of the apparatus is given in Fig. 1, with the magnetic field directed perpendicular to the drawing. The sulfur ion beam diameter at the target position was $\leq$6 mm, as determined by beam profile measurements taken 3 m downstream. Electrons and positrons generated by ions in the targets were separated in the nearly uniform ($\pm$ 3%) vertical magnetic field and transported 180° along circular arcs to one of two identical arrays of discrete detectors mounted on either side of the ion beam in the plane containing the chosen target. A schematic of the pair spectrometer, including views from the top and along the beam axis (z), is shown in Fig. 2. Projections of typical calculated trajectories are also shown there for 5 MeV/c electrons and positrons emitted at 0° and 20° with respect to the beam axis.

Each detector array was composed of 41 separate circular (2 cm dia.) silicon surface barrier detectors with depletion depths of 300 μm. Thin active depths minimized sensitivity to detection of γ-rays and permitted positrons to pass through without annihilation, delivering an average signal amplitude of ~105 keV. Detectors were arranged in five horizontal rows covering 52% of the available area as shown in Fig.

2a. The arrangement extended horizontally from 3 cm to 25 cm from the target center and vertically, 5.3 cm above and below the ion beam axis.

For forward emitted electrons or positrons, horizontal (x) displacement of the intercept point of a particle's trajectory with the detector plane is closely proportional to its momentum and is only weakly dependent on launch angle, due to first-order focusing in the plane of dispersion. Particle motion in the vertical (y) direction is unaffected by the magnetic field. Hence, the displacement of the detection position in the horizontal plane from the beam axis corresponds to positron or electron momentum while vertical (y) displacement corresponds to the vertical component of the transverse momentum (or the vertical component of the polar launch angle for a given total momentum.) The apparatus thus constitutes a 180°, homogeneous field, pair spectrometer.

For large polar angles, the dispersive plane focusing effect is weak. However, all electrons and positrons ejected with polar angles $\leq 20°$ would be focused to within the momentum resolution set by the 1.3 cm staggered horizontal spacing of the arrayed detectors. This fixed spacing gave a momentum resolution ($\Delta p/p$) varying from 33% at low momentum to 5.4% at high momentum for a given field setting. The limited vertical height of the array permitted full azimuthal collection only for limited ranges of polar angles which varied from 0-25° for the innermost (low momentum) detectors to 0-8° for the outermost (high momentum) detectors. Angular resolution, as determined by finite detector size and vertical spacing, varied from approximately $\pm 8°$ at low momentum to $\pm 2°$ at high momentum.

Two large scintillator veto detectors sensitive to minimum ionizing particles, each with a 6 cm diameter central hole, were mounted symmetrically about the beam axis 2 m upstream and downstream of the spectrometer (see Fig. 1). Signals from these

detectors were used to veto detector noise counts generated by any high energy particles accompanying the primary ions, but lying in an extended halo >3 cm beyond the main beam axis. A second veto signal was generated for similar halo and scattered high energy particles lying >2 mm and <4 cm from the beam axis, by a quartz Cerenkov active collimator located 5 m downstream, in the WA93 experiment (see Fig. 1).

Electron and positron counts were stored as functions of detector position for two settings of magnetic field (0.18 and 0.45 T) corresponding to detected momenta of 1.0–6.7 MeV/c and 2.5–17 MeV/c, respectively. Data were collected for targets of: 75 $\mu g/cm^2$ polypropylene $(CH_2)_x$; 180 $\mu g/cm^2$ Al; 4.9 mg/cm^2 Pd; and 0.6, 1.5, and 4.7 mg/cm^2 Au. The very thin targets ($<10^{-3}$ radiation length) were used to minimize backgrounds from direct Knock-On (KO) electrons and to avoid significant multiple Coulomb scattering (MCS) of low energy electrons and positrons.

Signals from the WA93 Zero Degree Calorimeter (ZDC)[17] were used in our experiment to identify, count, and provide timing for full energy projectile sulfur ions. The ZDC separately measured electromagnetic and hadronic stopping components in nine absorption lengths of uranium to obtain an energy resolution of $\sigma / E \approx 2\%$, just sufficient to discriminate against ions which have lost one nucleon in close collisions. These signals were employed for normalization and for coincidence measurements with positrons and/or electrons detected in our pair spectrometer.

Sulfur ions from the SPS were delivered in roughly uniform spills of 5.1 sec length with 10^5 to 10^6 ions per spill. For the 1.5 mg/cm^2 Au target, typical counting rates for 1–7 MeV/c positrons and electrons (primarily KO's) detected in coincidence with projectile ions were (1-10)/sec and (100-1000)/sec, respectively.

III. RESULTS AND DISCUSSION

A. Singles Measurements

Electrons and positrons from pairs formed in these peripheral collisions are emitted primarily in the forward direction. Instead of attempting to deconvolute measured distributions, we have mapped selected angular differential cross sections through the magnetic analyzing field to the detector plane and compared the resulting calculated distributions with the data. Using a computer simulation which incorporates effects of multiple Coulomb scattering (MCS), and assuming a simple exponential form for the angular cross section ($d\sigma/d\Omega_+ \sim \exp(-\theta/w)$, where θ is the polar angle measured from the beam axis), we have determined 1/e angular widths (w) which most closely reproduce the data, as a function of horizontal position (i.e., positron momentum). The exponential form for $d\sigma/d\Omega_+$ was chosen after reviewing several theoretical predictions[21,23] for expected angular distributions. Results of these simulation fits to the data are displayed in Fig. 3 for positrons from a 1.5 mg/cm^2 Au target. All other targets give similar results. Figure 3 also shows results for similar angular widths calculated in an exact Monte Carlo evaluation of the two-photon terms in lowest-order QED calculations for structureless nuclei described in Ref. 18, and hereafter referred to as MCQED. Widths from simulation fits to the data differ from the theoretical results by only ~1-2°, well within the experimental median angular resolution of 3° (excluding MCS angular smearing).

Since the angular distribution for positron emission is peaked so narrowly in the forward direction, the horizontal (x) intensity distribution on the detector array directly represents the momentum distribution. We have summed counts in sets of detectors grouped according to horizontal position and plot overlapping histograms of the resulting momentum distributions in Fig. 4, at the two field settings. The yields have been converted to cross sections and corrected for the fractions of positrons lying

outside the vertical acceptance of each detector group. These corrections were made assuming theoretical angular distributions with widths as presented in Fig. 3. Theoretical $d\sigma/dp_+$ cross sections are displayed in Fig. 4 as smooth curves. Results of First Born approximation calculations which employ Sommerfeld-Maue wave functions for the free electron and positron are displayed by the dashed line. To construct this curve, cross sections for 200 GeV protons and uranium targets have been interpolated from Fig. 4 of Ref. 19 and scaled according to Z_P^2 and Z_T^2 where Z_P and Z_T are the projectile and target nuclear charges, as directed in Ref. 18. We note that the First Born results underestimate the cross sections below ~3 MeV/c and overestimate them slightly above ~8 MeV/c. Results of MCQED calculations are indicated by the solid curve. Agreement is remarkably good up to ~4 MeV/c. At higher momenta MCQED gives cross sections as much as 75% higher than the measurements. Linear extrapolation of the First Born cross sections gives a cross section of about 83 barns integrated over 1-17 MeV/c. The corresponding MCQED result is 98 barns. The measured cross section is 85 ± 22 barns, where the error includes statistical and background correction errors and estimated uncertainties in detection and acquisition efficiencies.

To examine the dependence of pair production on target nuclear charge Z_T, we have integrated singles positron yields over 2.5–17 MeV/c for targets of Al, Pd, and Au and plotted the resulting relative partial cross sections against Z_T. The results are displayed in Fig. 6. The solid line in the figure represents a least squares fit proportional to Z_T^n to these data. The fit gives $n = 1.99 \pm 0.02$. The lower and upper smooth dashed curves represent n values of 1.95 and 2.05, respectively. Cross sections are expected to scale as Z_T^2 by all known first-order theories. Deviations from Z_T^2 scaling might indicate importance of higher order terms arising from positron-target interaction.[19]

B. Electron-Positron Coincidence Measurements

Coincidence electron-positron measurements were primarily restricted to gold targets. Only very low statistics coincidence data were obtained for the lighter targets and results reported here will concentrate on the gold target measurements. Doubly differential yields have been obtained by sorting event data into coincidence counts as functions of various parameters calculated from the (41 x 41) possible pairs of detector positions. To obtain cross sections, corrections have been made for variations in detector efficiencies and for estimated fractions of detector intercepted electrons and positrons, according to assumed extended angular distributions as indicated for singles positrons (see Fig. 3).

As noted for the singles data, the vertical displacement of a detected electron is approximately proportional to the vertical component (p_y) of its transverse momentum. We have sorted event data to determine the relative intensity distributions as a function of pair ($p_{y+} + p_{y-}$) transverse momenta and present the results in Fig. 7. Observed p_y distributions are plotted for both magnetic field settings representing measured positron (or electron) momenta ranges of 1–7 MeV/c and 2.5–17 MeV/c, respectively. Both low and high field p_y distributions peak at zero and fall rapidly, with more than 80% of all observed pairs having $p_y \leq 1$ MeV/c. By symmetry, the horizontal component (p_x) of the transverse momentum should have the same intensity distribution. We conclude that pair transverse momenta are small and increase only weakly for higher positron momenta (at least up to ~17 MeV/c), and that measured longitudinal (z) momentum distributions therefore well represent the total pair momentum, since the small transverse components approximately cancel..

Figure 8 displays results for $(d^2\sigma/dp_+dp_-)$ for positrons from a gold target in coincidence with the 1–7 MeV/c electrons which were simultaneously detected by the full electron detector array at the low magnetic field setting. Comparison with the singles positron cross sections in Fig. 5 shows that the momentum distributions are nearly the same, suggesting therefore, that positron momenta are almost entirely independent of electron momentum. Tighter cuts on the momenta of coincident electrons yield the same general result. Cross sections $d^2\sigma/dp_+dp_-$ for positrons and for electrons are compared in Fig. 9, where the momentum for the coincident particle has been limited in the sort of the data to 3 – 6 MeV/c. The smooth curves indicate first-order Born approximation results of Ref. 18, taken from Figs. 1 and 2, interpolated to $\gamma = 215$ (200 GeV/nucleon) and scaled as $Z_p^2 Z_T^2$. We note that the calculated cross sections exceed the measured values by ~80%, and that measured $d^2\sigma/dp_+dp_-$ decrease systematically with increasing positron or electron momentum, unlike calculated values which exhibit maxima near 3 MeV/c. The only substantial difference between the measured electron and positron spectra displayed in Fig. 9, is a slight shift in the electron distribution toward low momentum. For momenta ≤4 MeV/c, the yield of electrons exceeds that of positrons by 23%. The excess could be explained by coincidences (random and correlated) with low momentum KO electrons, where singles rates (see Fig. 5) are 5 to 100 times larger than for positrons and hence, for pair-generated electrons. However, the random positron-KO electron coincidence fraction is estimated to be very small for the thin targets used here. A typical randoms/reals fraction calculated from measured singles rates and from the time window defining a coincidence is 10^{-2}, or ~1%. Correlated coincidences between positrons and KO electrons could also occur because of secondary KO production by the pair-producing ion, either in ion-electron collisions within the same atom participating in pair production event or in another collision by the same ion in traversing the remaining thickness of the target foil. For typical thickness gold targets, the latter is just the

measured (1-17 MeV/c) KO yield/ion which is $\leq 10^{-2}$. We estimate from Born approximation calculations of (primarily K-shell) target ionization that the former process will occur ~1% of the time, with less than half of these being detected. Therefore, the sum of random and correlated coincidences between positrons and KO electrons should amount to less than 2% of the real pair coincidences.

The difference between the positron and electron distributions may be attributed instead to a real charge-dependent effect due to the sign difference of the Coulomb potential at the origin of the pair. The $d^2\sigma/dp_+dp_-$ weighted average kinetic energies taken from the data in Fig. 8 are 4.21 and 3.87 MeV, respectively, for 1–17 MeV/c positrons and electrons. If we interpret in a purely classical picture this (0.34 MeV) shift in the average kinetic energy as arising from a potential energy difference experienced by the oppositely charged particles at the pair origin, then a rough approximation of the mean distance <b> to the gold target nucleus (neglecting screening and the sulfur ion's field) gives $\langle b \rangle \approx 700$ fm or $\sim 2\lambda_c$, which is consistent with impact parameters expected to be important according to equivalent photon methods.[26] (The 1–17-MeV/c electrons and positrons are localized to $\ll \lambda_c$ according to the uncertainty principle.)

We have also investigated the distribution of pair total kinetic energy, by converting the separate momenta of electrons and positrons forming detected pairs to kinetic energies (ε_+ and ε_-). The energies have been combined to give total pair energies $\varepsilon = \varepsilon_+ + \varepsilon_-$, and the corresponding corrected counts have been grouped to give intensity distributions, with the ranges of either component limited by the energies (momenta) covered by all detectors at each field setting. To correct for sorting biases arising from incomplete coverage of all possible momenta (0–17 MeV/c) for the pairs of particles, we have continued our measured data by fitting to a double exponential function as $d^2\sigma / dp_+dp_- \sim e^{-\alpha(p_+ + p_-)} + f\ e^{-\beta(p_+ + p_-)}$, where α, β, and f are fitted

parameters applicable for all data. The original data plus fitted regions were then sorted with respect to pair kinetic energy ε. Sorts were performed assuming exponential $d^2\sigma/dp_+dp_-$ extending all the way to zero p_+ and p_- and using a more physically reasonable model in which $d^2\sigma/dp_+dp_-$ falls smoothly from the measured values obtained at the lowest measured p_+ and p_- to zero at zero p_+ and p_-. Results are shown in Fig. 10 for the relative yields of pairs as a function of ε. We note that the yields fall nearly exponentially with no indication of a maximum above 2 MeV, and that 50% of all observed pairs have total kinetic energies below 4 MeV. Theory typically predicts a downturn in the cross section below ~4 MeV.[20]

These same energy data have been analyzed in the manner described above to determine the fraction of total pair kinetic energy carried away by the positron. Fig. 11 shows the probability distribution for energy sharing measured for pairs covered in the two field settings. The error bars represent statistical and efficiency uncertainties for the ratios of binned counts and effects of uncertainties in the fits giving the calculated counts expected in the extended regions of p_+ and p_-. It appears that all modes of partitioning of the energy available are nearly equal probable. However, there is a weak tendency for positrons to carry slightly more kinetic energy than coincident electrons, consistent with our observations of $p_- = 3$–6 MeV/c.

In summary, the observed projected angular distributions for low energy positrons are consistent with forward peaked emission with the differential cross section $(d\sigma/d\Omega_+)$ falling to 1/e of its peak value for polar angles varying from ~12° at 1 MeV/c to ~4° at 14 MeV/c. This distribution of angular widths agrees with MCQED calculations for differential cross sections. The positron momentum distribution is peaked below our detection limit of 1 MeV/c and falls to half its observed maximum at ~5 MeV/c. First Born calculations tend to underestimate the measured cross section at low momenta,

being lower by as much as 35% below 2 MeV/c. MCQED calculations agree well at low momenta, but overestimate the observed cross sections by as much as 80% above 8 MeV/c. Measured cross sections decrease faster at higher momenta than predicted by either calculation. The 1–17-MeV/c positron yield for 6.4-TeV sulfur on gold, corrected for detector efficiencies, integrated over the momentum and angular acceptances set by the detector array dimensions and the magnetic analyzing field, gives an observed cross section of 71 barns. Correction for partial angular acceptance versus momentum, based on observed vertical (y) angular distributions within the detection window, raises the measured total cross section to 85 barns with an estimated error of ±25%. The corresponding MCQED value is 98 barns out of a total, integrated over all momenta, of 140 barns. Finally, the measured cross sections vary with target nuclear charge as Z_T^2 as predicted by all lowest order calculations, and relative differential cross sections $d\sigma/dp_+$ are indistinguishable for Al, Pd, and Au targets.

From coincident measurements of positrons and electrons, the pair transverse momentum and total kinetic energy distributions have been determined. Within limited statistics data for Al and Pd, these distributions are insensitive to target Z_T. Pair transverse momenta are small (<1 MeV/c) implying that the electron and positron are emitted in the plane of the projectile ion. The pair differential cross-section $d\sigma/d\varepsilon$ falls nearly exponentially from 2–30 MeV, with no indication of a non-zero threshold or maximum above 2 MeV. Momentum distributions for positrons and electrons detected as pairs are similar, with a small relative shift toward lower momenta (kinetic energies) noted for the electrons. Interpreted as a potential difference at the origin, this shift suggests that important impact parameters lie near ~2 $\lambda\!\!\!^{-}_c$ for production of low energy pairs. The available excess kinetic energy of the pair is shared between the electron and positron such that all modes are nearly equally populated.

The relatively good agreement between measured $d\sigma/dp_+$ and lowest order perturbative calculations is expected for 6.4 TeV $S^{16+} + Z_T$ (Z_T = 13, 46, and 79), where $Z\alpha \ll 1$, and the probability of producing an electron pair is expected to be small at all impact parameters. It should be noted that this is in contrast to the recent results of experiments[37,38] at lower energies for uranium and lanthanum projectiles, where perturbative calculations for electron-capture of the pair-produced electrons apparently fails. At higher energies and for the heaviest projectiles, perturbative treatments may also fail, since low order perturbation terms give probabilities for single pair formation which exceed unity at sufficiently small impact parameters. Several theoretical treatments have concluded that multiple pairs will be formed in single close collisions, with some considerable disagreement among the calculations as to the relative strengths of the multiple pair forming channels.[5,7,8,13] Using perturbation theory values for the probabilities of producing a single pair, several authors[5,8] predict that the number distribution of multiple pairs produced will follow a Poisson distribution. Analysis of non-perturbation expressions for N-pair creation have lead to the same distribution with significant disagreement for absolute cross sections.[12] We will test these predictions in experiments using 33 TeV (γ=172) Pb^{82+} ions at the CERN SPS accelerator, expected to become available in late 1994.

ACKNOWLEDGEMENTS

This research was sponsored by the U. S. Department of Energy, Office of Basic Energy Sciences, Division of Chemical Sciences under Contract No. DE-AC05-84OR21400 with Martin Marietta Energy Systems, Inc.

REFERENCES

1. P. F. Dittner, S. Datz, P. D. Miller, C. D. Moak, P. H. Stelson, C. Bottcher, W. B. Dress, G. D. Alton, and N. Neskovic, Phys. Rev. Lett. **51**, 31 (1983).

2. C. R. Vane, S. Datz, P. F. Dittner, H. F. Krause, C. Bottcher, M. Strayer, R. Schuch, H. Gao, and R. Hutton, Phys. Rev. Lett. **69**, 1911 (1992).

3. C. R. Vane, S. Datz, P. F. Dittner, H. F. Krause, R. Schuch, H. Gao, and R. Hutton, Phys. Rev. A (1994), in press.

4. C. Bottcher and M. R. Strayer, Phys. Rev. D **39**, 1330 (1989).

5. M. J. Rhoades-Brown and J. Weneser, Phys. Rev. A **44**, 330 (1991).

6. F. Decker, Phys. Rev. A **44**, 2883 (1991); F. Decker and J. Eichler, Phys. Rev. A **45**, 3343 (1992).

7. K. Rumrich, K. Momberger, G. Soff, W. Greiner, N. Grün, and W. Scheid, Phys. Rev. Lett. **66**, 2613 (1991).

8. G. Baur and C. A. Bertulani, Phys. Rev. C **35**, 836 (1987); G. Baur, Phys. Rev. A **42**, 5736 (1990).

9. J. Eichler, Phys. Rep. **193**, 167 (1990) – review of theoretical progress to 1990.

10. P. B. Eby, Phys. Rev. A **43**, 2258 (1991) and Phys. Rev. A **39**, 2374 (1989).

11. K. Kajantie, M. Kataja, L. McLevran, and P. V. Ruuskanen, Phys. Rev. D **34**, 811 (1986); K. Kajantie, J. Kapusta, L. McLevran, and A. Mekjian, ibid.**34**, 2746 (1986).

12. C. Best, W. Greiner, and G. Soff, Phys. Rev. A **46**, 261 (1992).

13. J. C. Wells, V. E. Oberacker, A. S. Umar, C. Bottcher, M. R. Strayer, J.-S. Wu, and G. Plunien, Phys. Rev. A **45**, 6296 (1992).

14. H. Gould, in "Atomic Theory Workshop on Relativistic and QED Effects in Heavy Atoms", Hugh P. Kelly and Yong-ki Kim, eds. (AIP Conf. Proc. 136), (AIP, New York,1985).

15. C. Bottcher and M. R. Strayer, in "Physics of Strong Fields", W. Greiner, ed. (NATO ASI Ser. B Vol 153) (Plenum, New York, 1987), pg. 629.

16. E. Teller, Nucl. Instrum. Meth. Phys. Res. **B24/25**, 3 (1987).

17. G. R. Young, et al., Nucl. Instrum. Meth.**A279**, 503 (1989)

18. K. F. Weizsäcker, Z. Phys. **88**, 612 (1934).

19. D. C. Ionescu and J. Eichler, Phys. Rev. A **48**, 1176 (1993).

20. For example, see Fig. 6 of Ref. 10.

Figure Captions

Fig. 1. Schematic of experimental apparatus showing veto detectors, magnetic pair spectrometer, and ion calorimeter detector (ZDC).

Fig. 2. Schematic of pair spectrometer. (a) End view along beam axis showing target and detector arrays. (b) Top view showing detectors in mid-plane row and sample trajectories for 5 MeV/c positrons and electrons emitted at 0° and 20° to indicate effects of dispersive plane focussing.

Fig. 3. Angular 1/e widths for $d\sigma/d\Omega_+$ plotted as a function of positron momentum for 6.4 TeV S + Au. Data points (o) are results of simulation fits to measured vertical intensity distributions as described in the text. Error bars indicate observed fitting uncertainty dominated by experimental angular resolution set by detector size. Theoretical results (—) are from MCQED calculations.

Fig. 4. Measured positron singles cross sections $d\sigma/dp_+$ compared with theoretical results. Overlapping solid line histograms are measured cross sections for field settings of 0.18 and 0.45 Tesla, corrected for incomplete detection of the full angular emission distributions as described in the text. Smooth curves represent results of MCQED calculations (——) and interpolations of scaled First Born calculation results (- - -) given in Ref. 23.

Fig. 5. Measured yields of electrons and positrons from a 1.5 mg/cm^2 Au target detected independently, but in coincidence with 6.4 TeV sulfur ions. The solid curve displays results of Born approximation calculations for binary ion-electron collisions described in Ref. 35.

Fig. 6. Measured yields of positrons/ion/target atom, for Al, Pd, and Au, plotted as a function of target nuclear charge. Detected energy range is 2.5 – 17 MeV. Error bars represent statistical errors and variations in several

Figure Captions (contd)

measurements for a given target element. Power law fit to the data gives $Z_T^{1.99 \pm 0.02}$ as depicted by the solid curve. Dashed curves indicate n = 1.95 and 2.05.

Fig. 7. Transverse vertical momentum ($p_{y+} + p_{y-}$) distributions for detected electron-positron pairs at the two magnetic field settings. Target is gold. Curve added to guide the eye.

Fig. 8. Doubly differential cross sections $d^2\sigma/dp_+dp_-$ for positrons detected in coincidence with the full momentum range of intercepted electrons at the low magnetic field setting. Solid curve shows relative variation of $d\sigma/dp_+$ taken from data of Fig. 4. Target is 1.5 mg/cm^2 Au.

Fig. 9. Doubly differential cross sections $d^2\sigma/dp_+dp_-$ for positrons (a) and for electrons (b). Momentum range for the coincident pair partner is 3–6 MeV/c in each case. Target is 1.5 mg/cm^2 Au.

Fig. 10. Relative differential cross section $d\sigma/d\varepsilon$ for pairs of electrons and positrons. ε is the sum of positron and electron kinetic energies.

Fig. 11. Probability distribution for energy partitioning between the coincident (1–17 MeV) positrons and electrons forming pairs with energy distribution shown in Fig. 10.

ORNL DWG 93-11594R

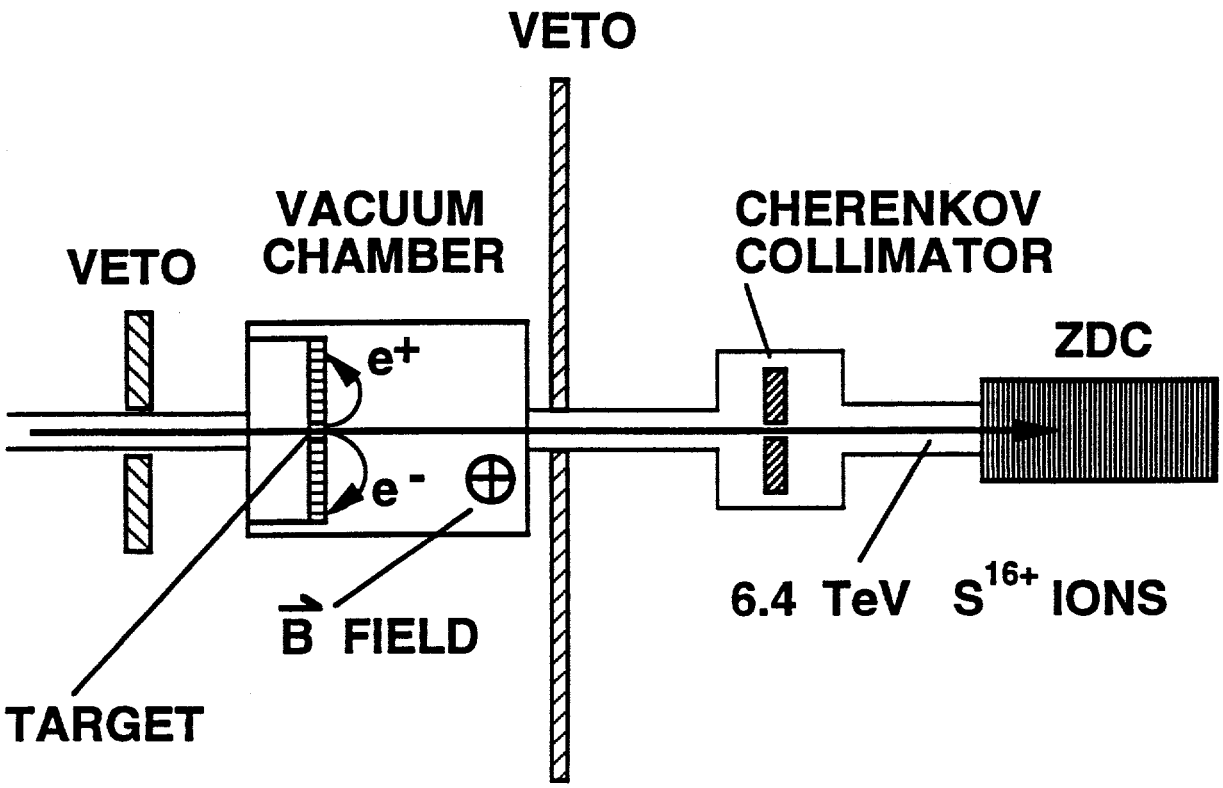

Figure 1

ORNL DWG 93-11595R

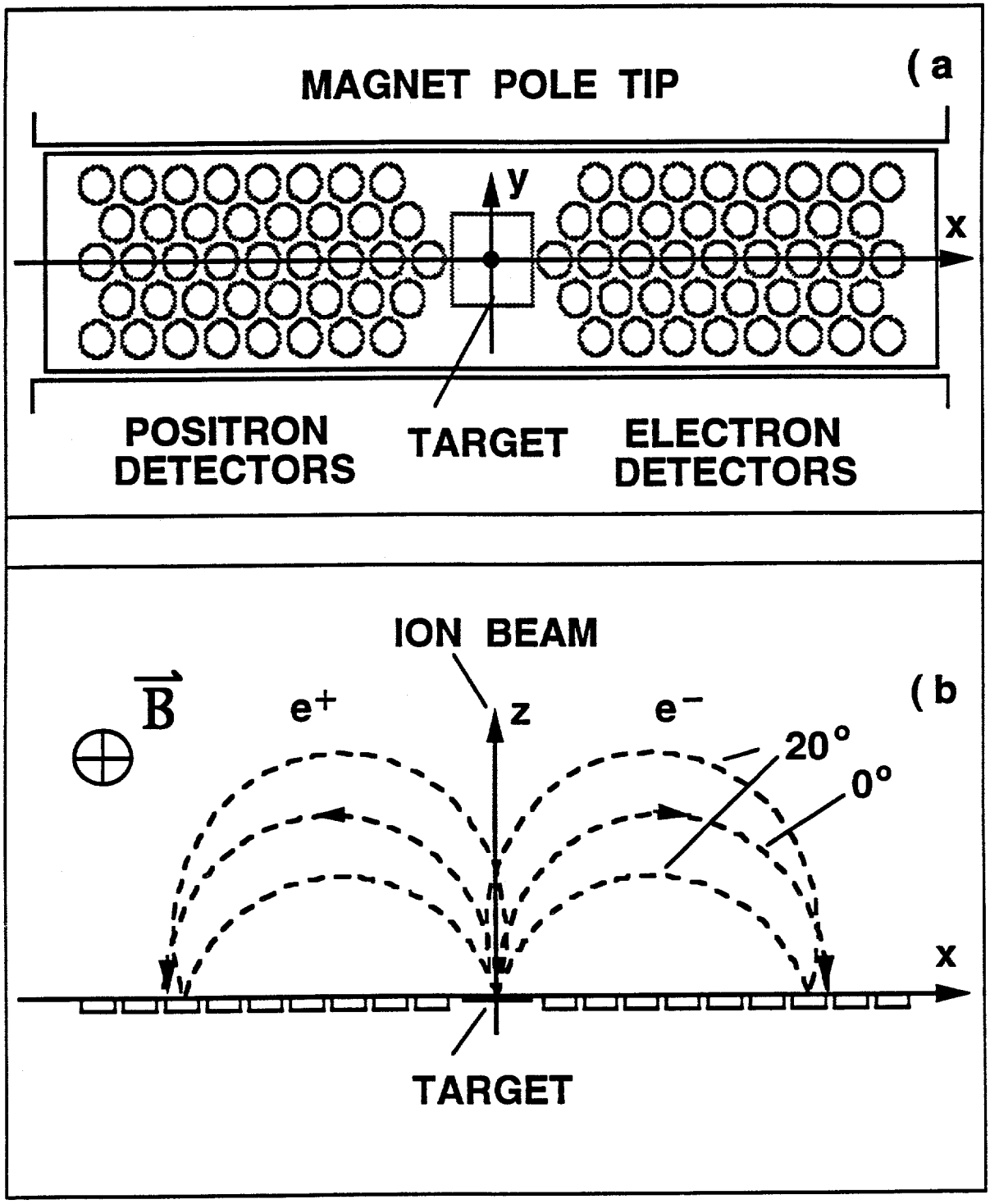

Figure 2

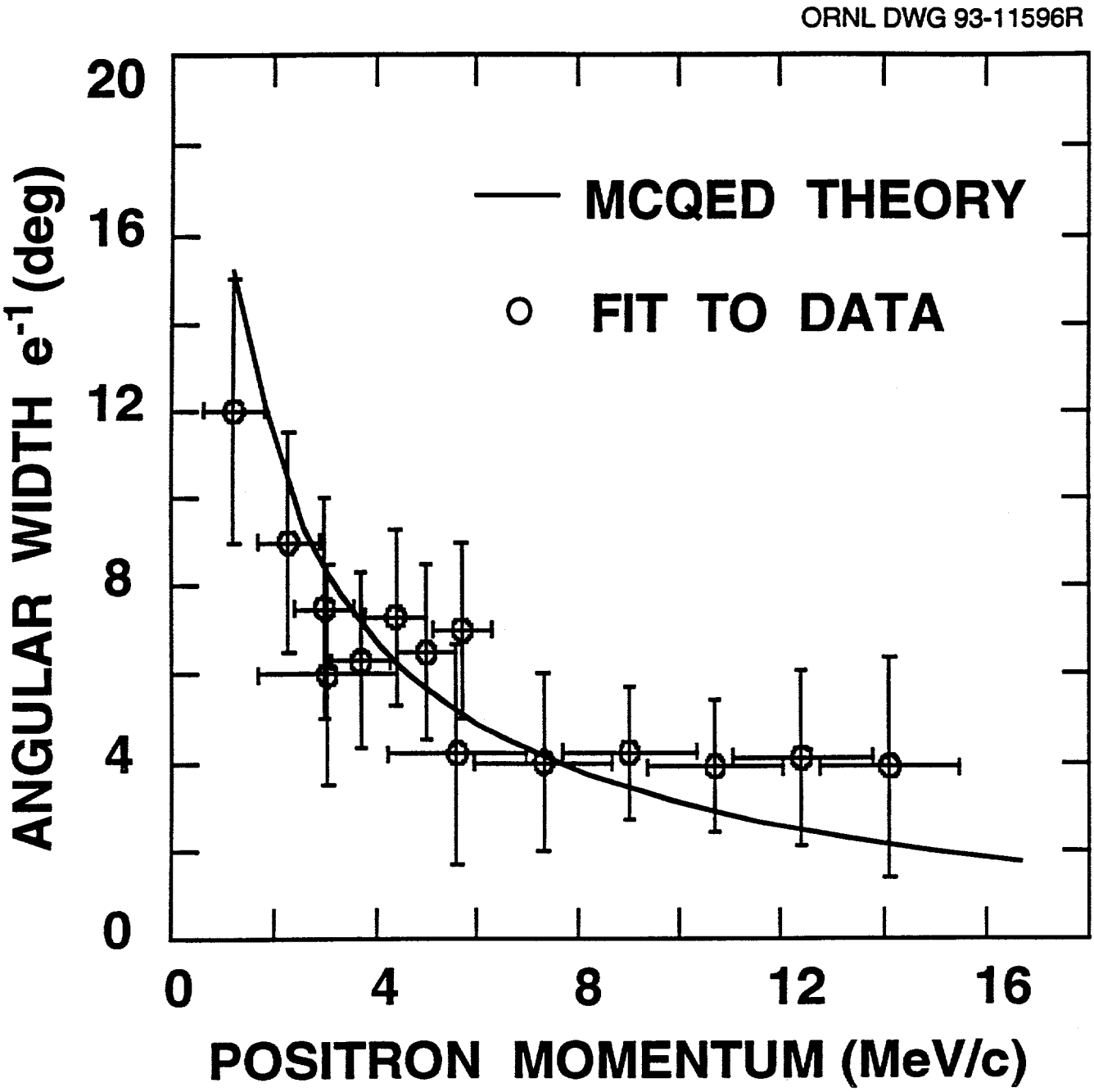
ORNL DWG 93-11596R
20
16
12
8
4
0
ANGULAR WIDTH e-1 (deg)
MCQED THEORY
FIT TO DATA
0
4
8
12
16
POSITRON MOMENTUM (MeV/c)

Figure 3

ORNL DWG 93-11597R

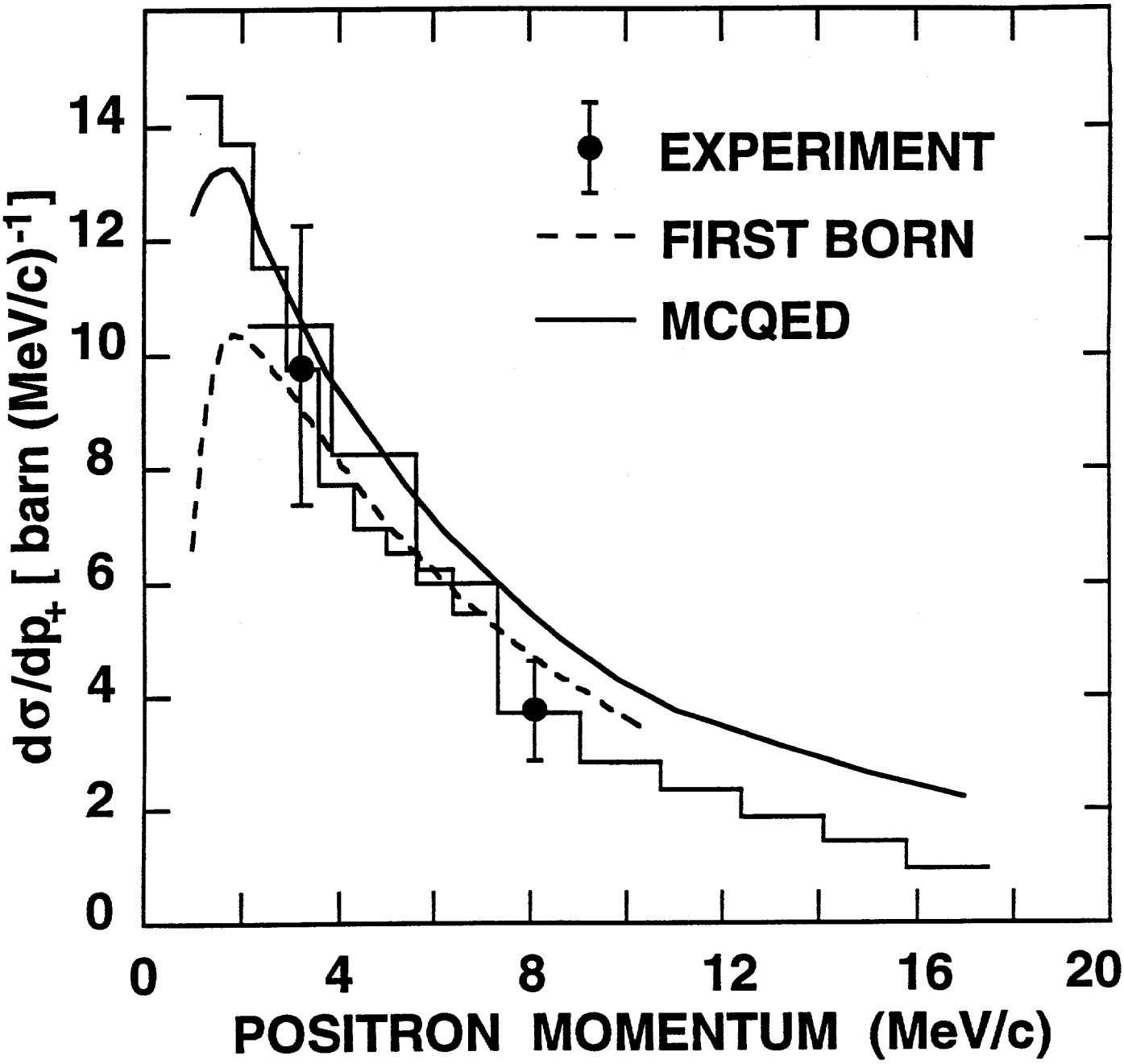

Figure 4

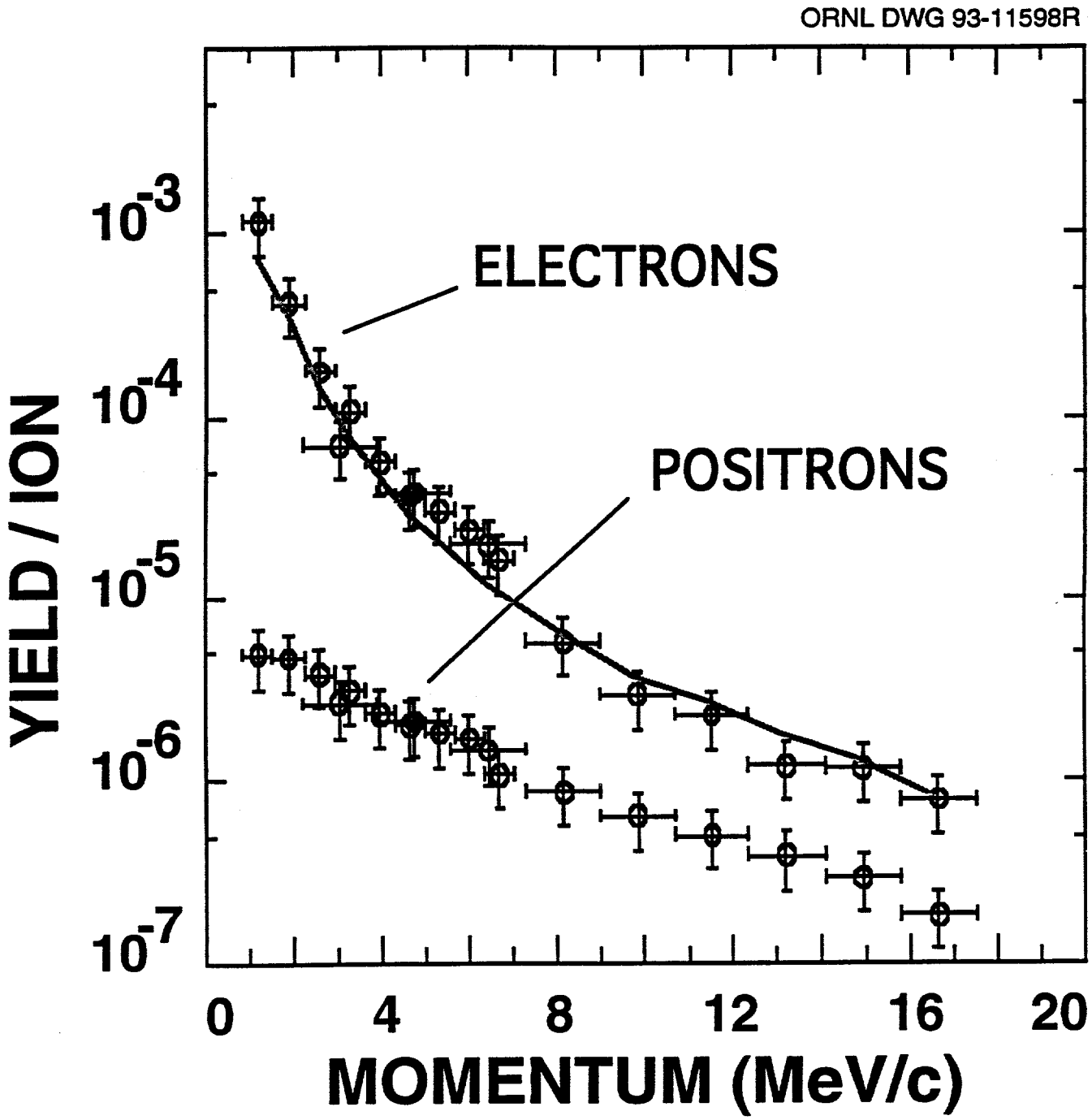
ORNL DWG 93-11598R
YIELD / ION
10^{-3}
10^{-4}
10^{-5}
10^{-6}
10^{-7}
ELECTRONS
POSITRONS
0
4
8
12
16
20
MOMENTUM (MeV/c)

Figure 5

ORNL DWG 93-11599R

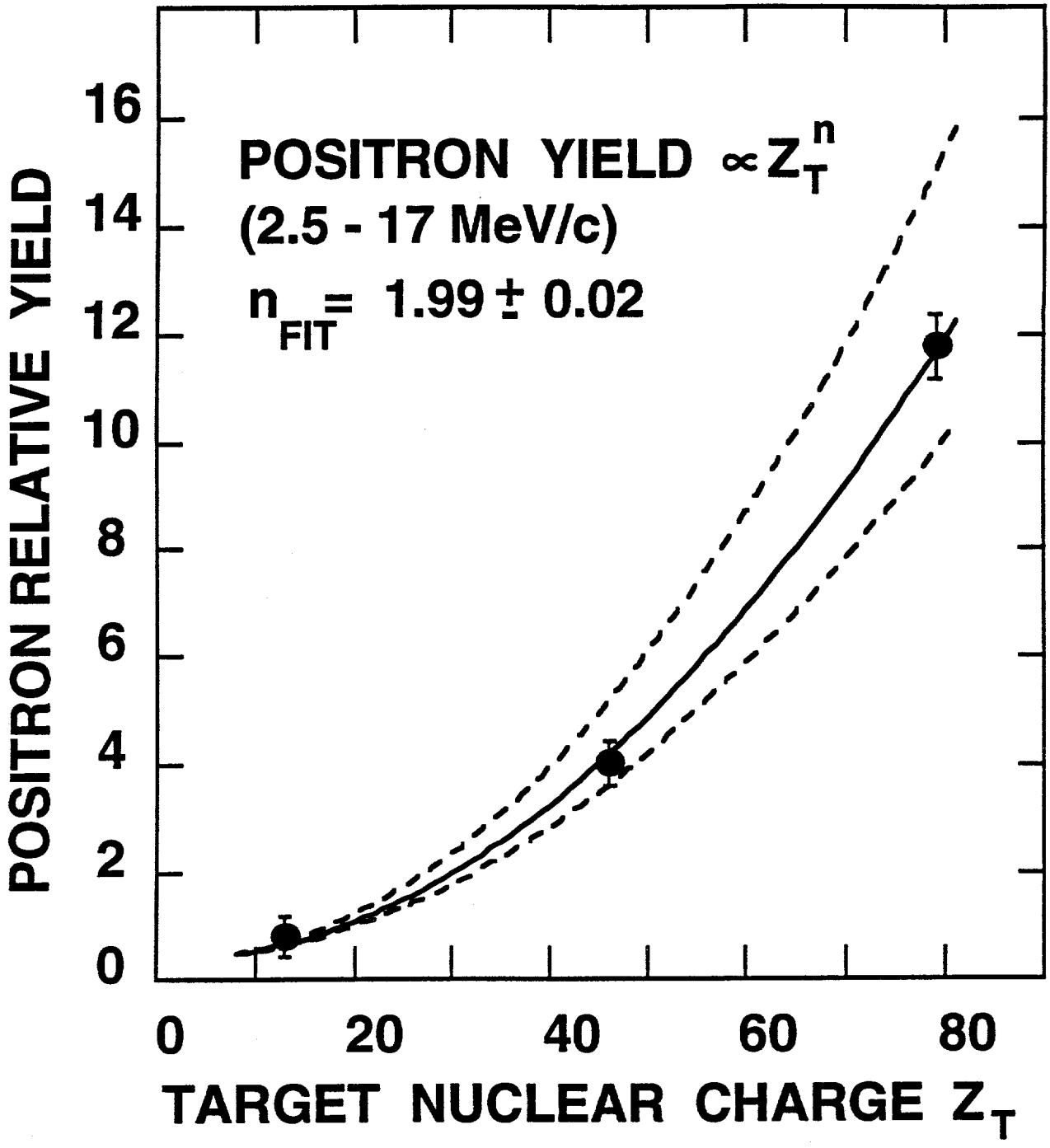

Figure 6

ORNL DWG 93-11603R

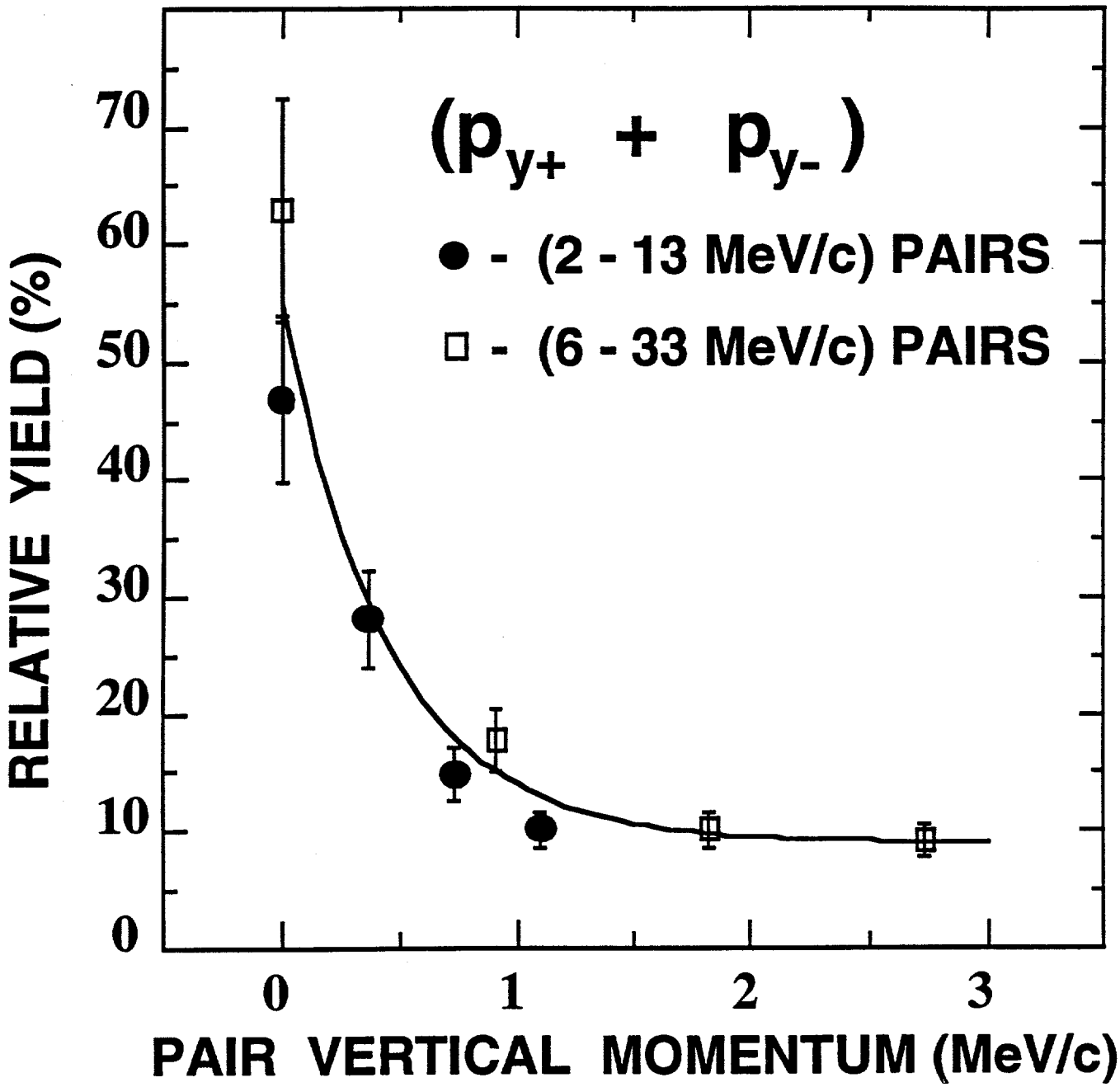

Figure 7

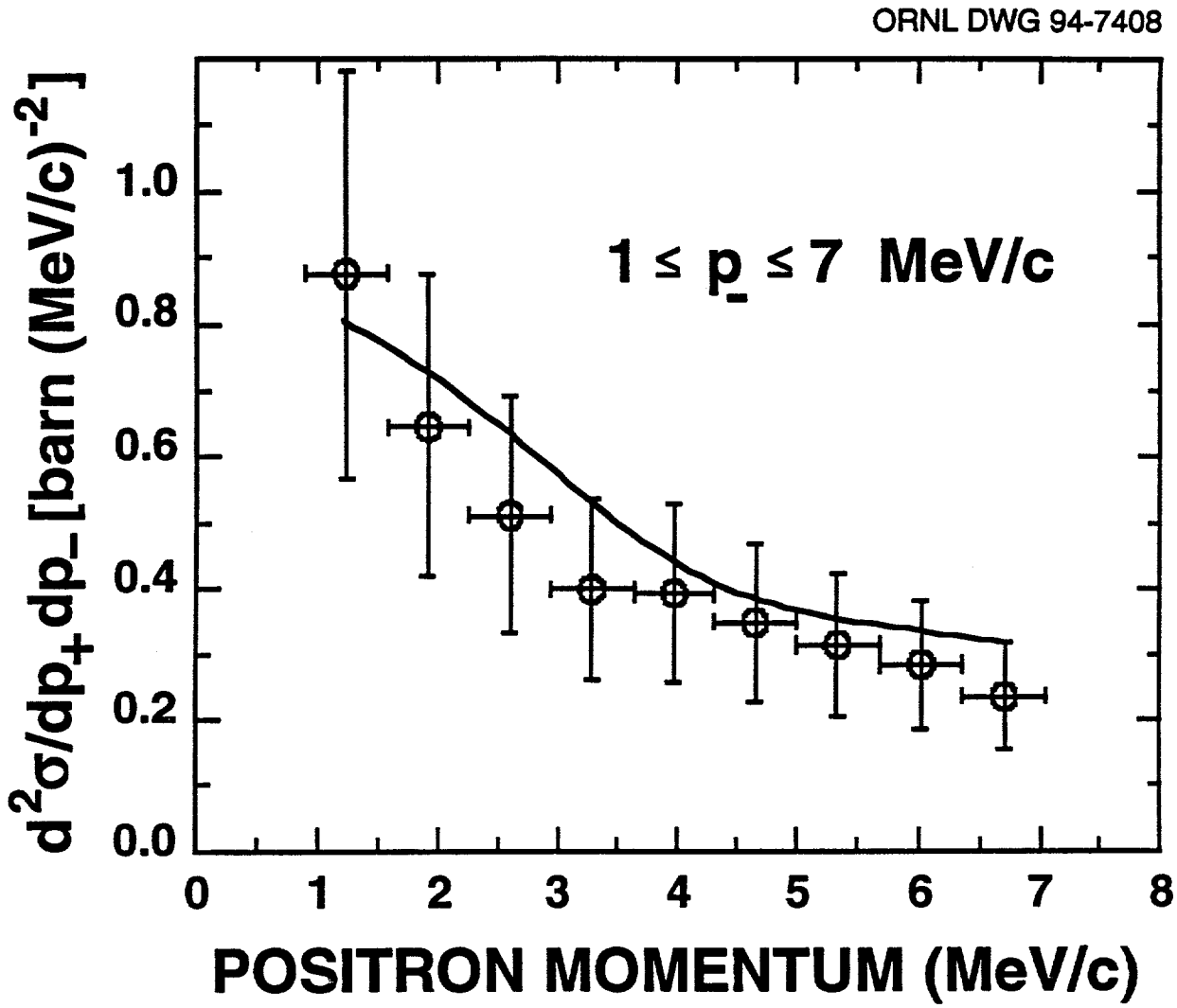
ORNL DWG 94-7408
$d^2\sigma/dp_+dp_-$ [barn (MeV/c)$^{-2}$]
1.0
0.8
0.6
0.4
0.2
0.0
$1 \leq p_- \leq 7$ MeV/c
0
1
2
3
4
5
6
7
8
POSITRON MOMENTUM (MeV/c)

Figure 8

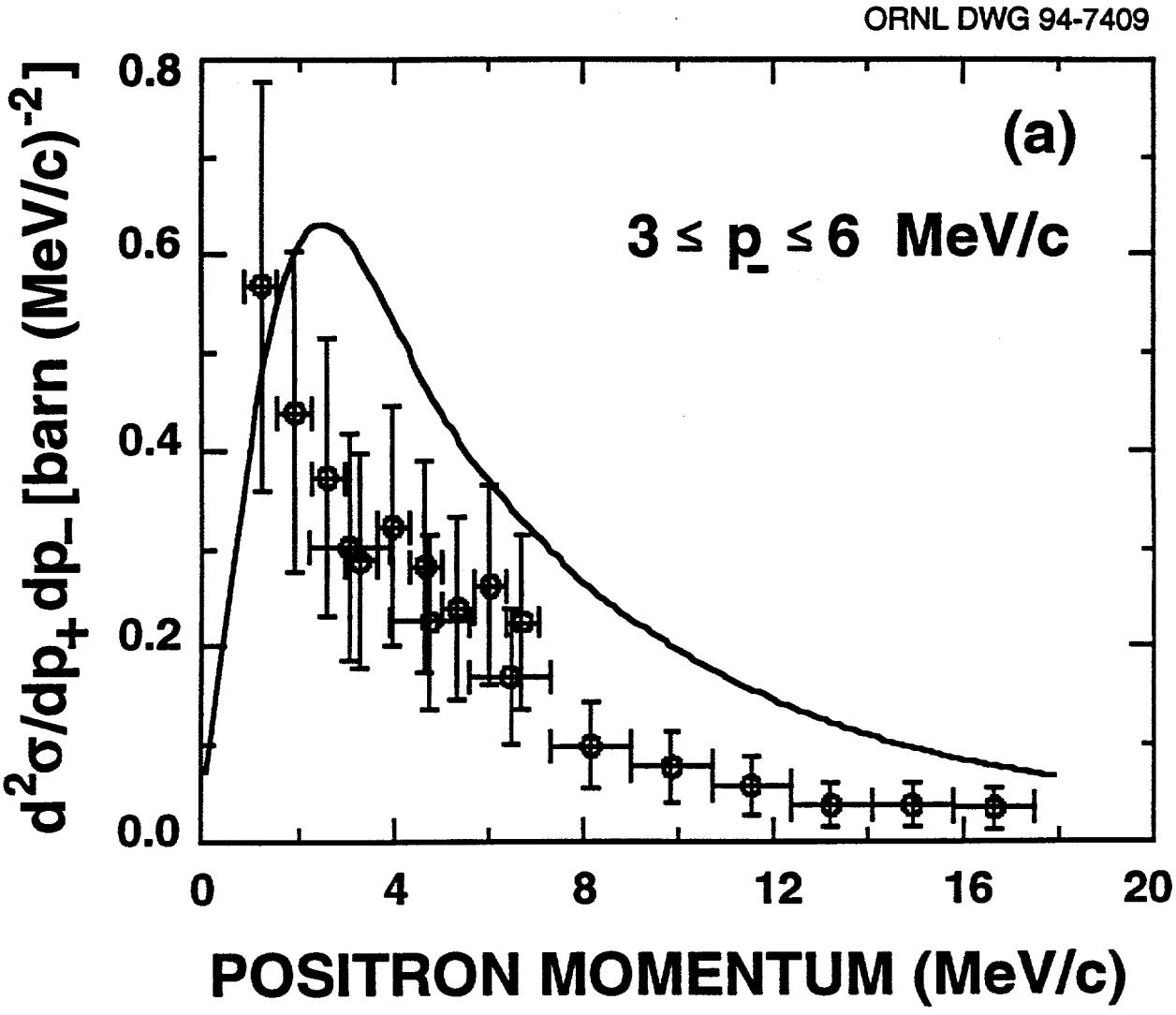
ORNL DWG 94-7409
(a)
3 ≤ p_ ≤ 6 MeV/c
d²σ/dp₊dp₋ [barn (MeV/c)⁻²]
0.0
0.2
0.4
0.6
0.8
0
4
8
12
16
20
POSITRON MOMENTUM (MeV/c)

Figure 9 (a)

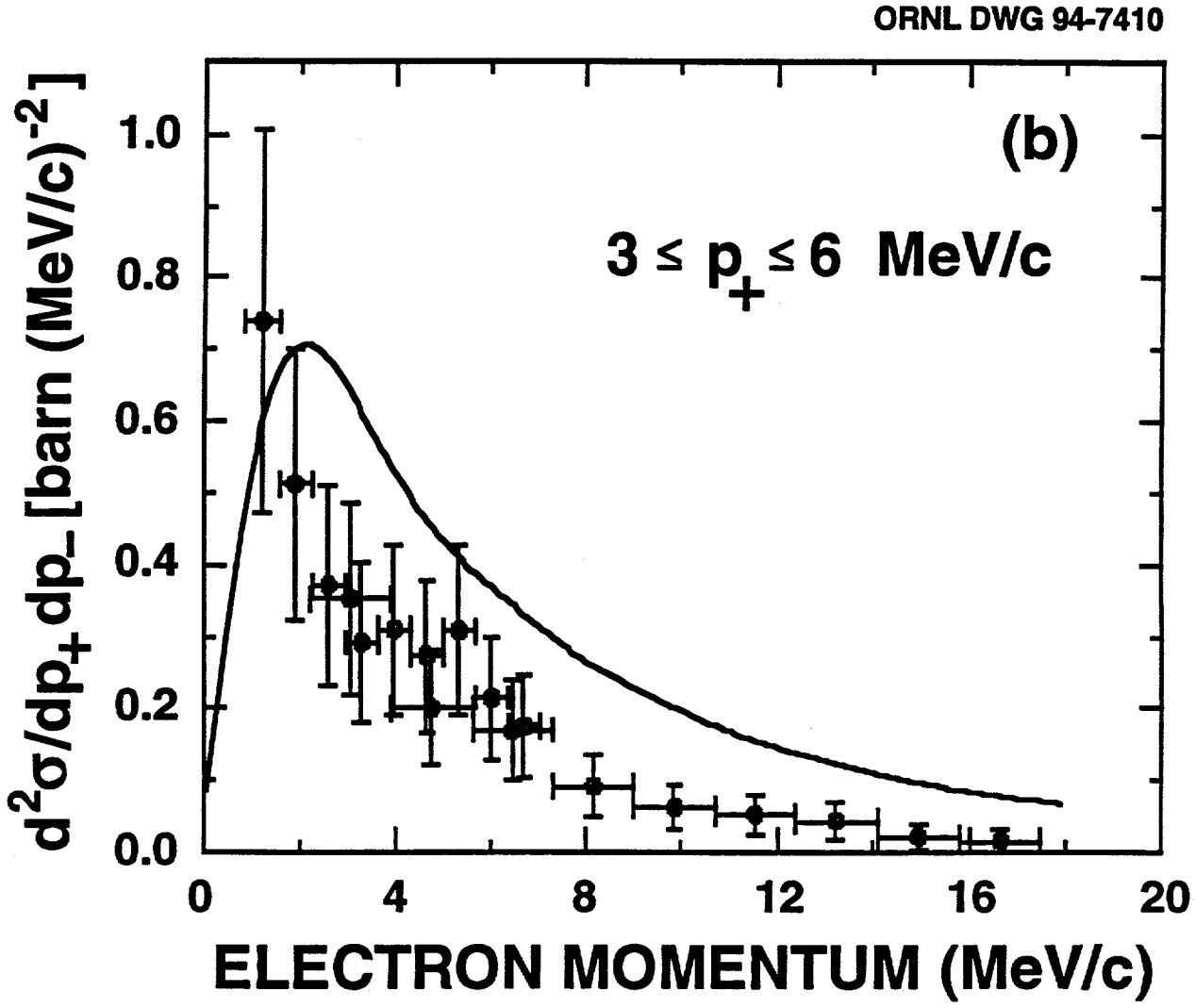
ORNL DWG 94-7410
(b)
3 ≤ p+ ≤ 6 MeV/c
d²σ/dp+dp- [barn (MeV/c)⁻²]
1.0
0.8
0.6
0.4
0.2
0.0
0
4
8
12
16
20
ELECTRON MOMENTUM (MeV/c)

Figure 9 (b)

ORNL DWG 94-7411

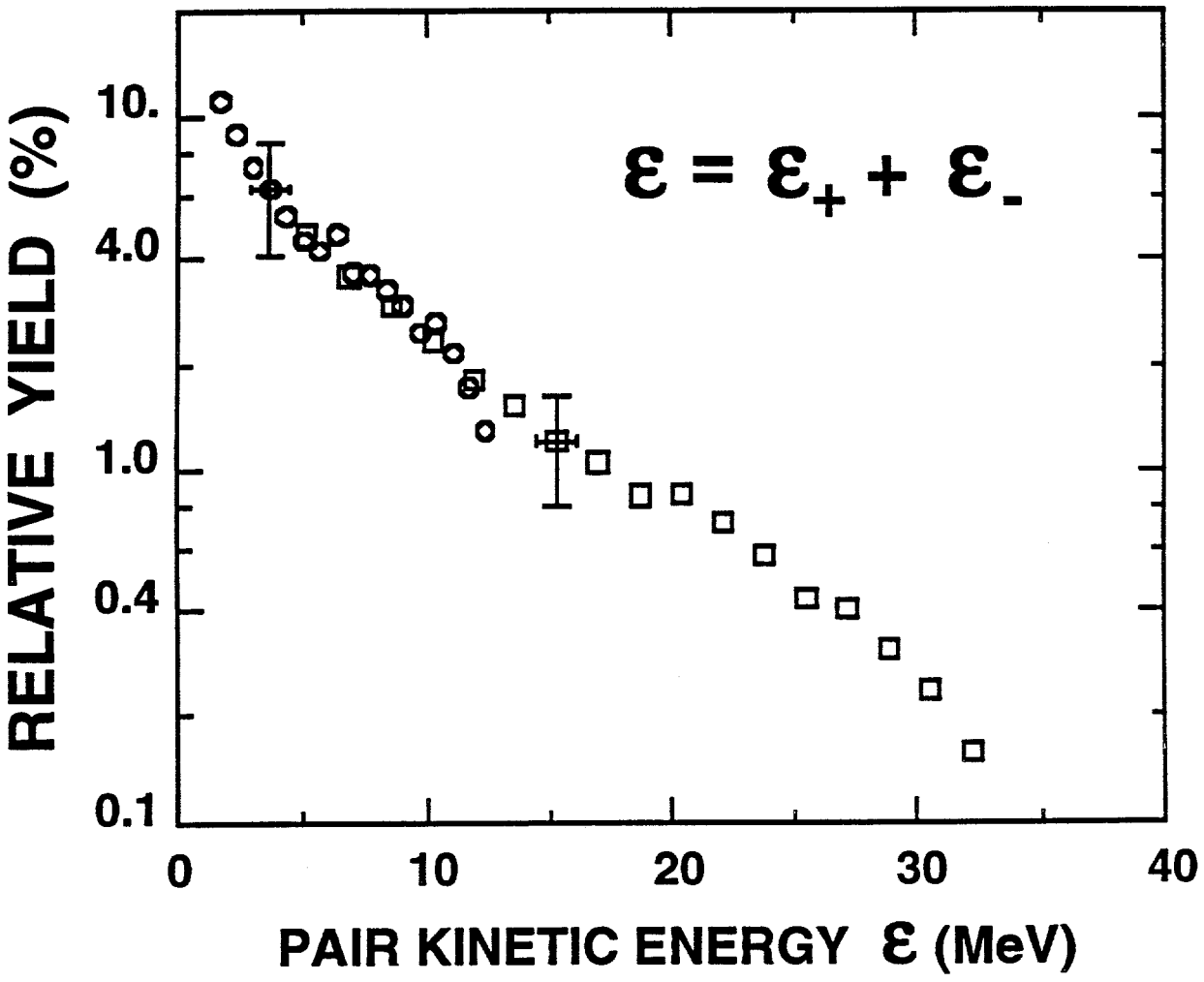

Figure 10

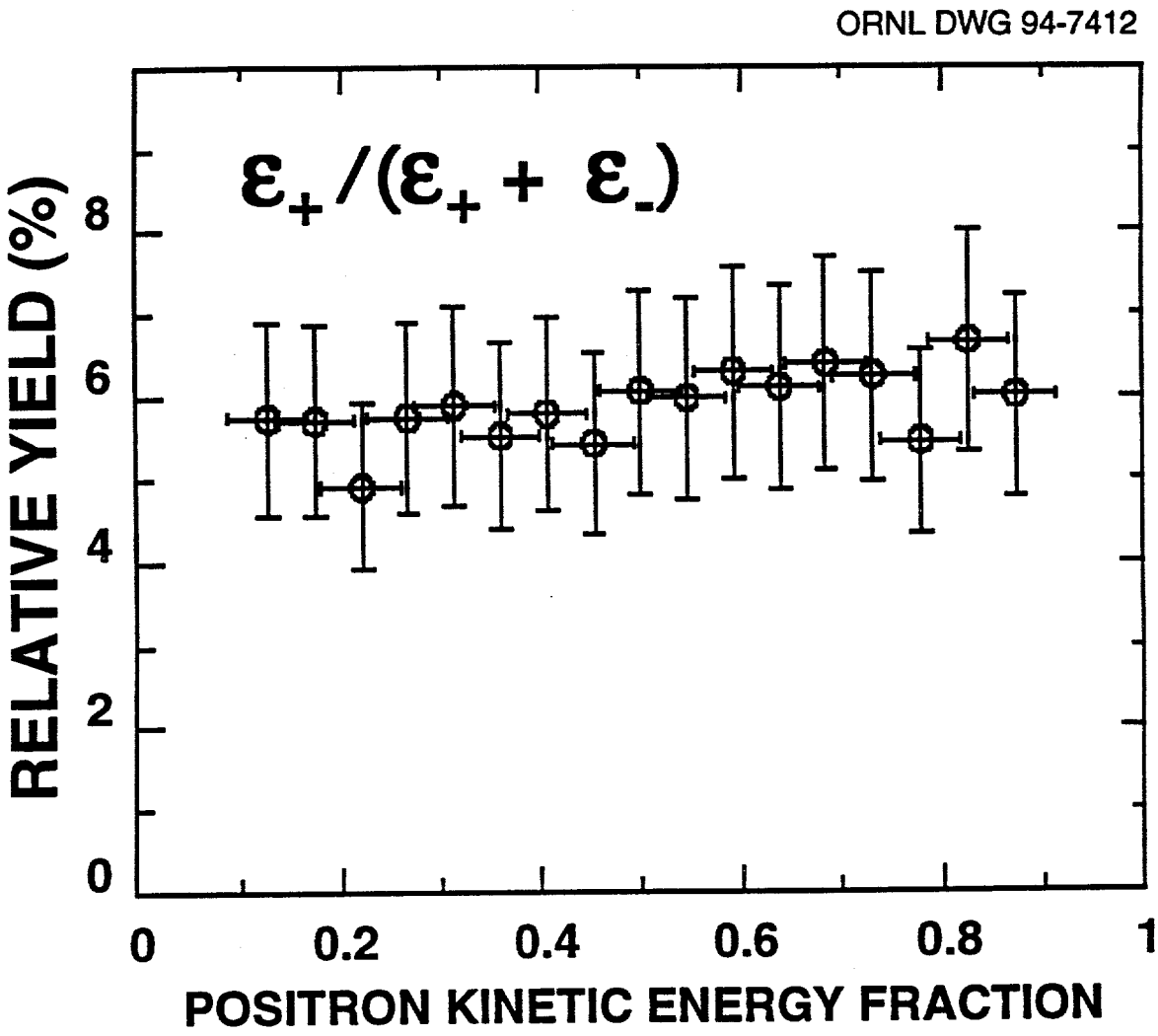
ORNL DWG 94-7412
$\varepsilon_+/(\varepsilon_+ + \varepsilon_-)$
RELATIVE YIELD (%)
0
2
4
6
8
0
0.2
0.4
0.6
0.8
1
POSITRON KINETIC ENERGY FRACTION

Figure 11